FRONTIERS OF PHYSICS

RESEARCH ARTICLE
Volume 20 / Issue 3 / 032204 / 2025

Holevo Cramér–Rao bound for multi-parameter estimation in nonlinear interferometers

Mengyao Zhou[1], Hongmei Ma[2], Liqing Chen[1,†], Weiping Zhang[3,4,5,6], Chun-Hua Yuan[1,‡]

1 State Key Laboratory of Precision Spectroscopy, Quantum Institute for Light and Atoms, School of Physics and Electronic Science, East China Normal University, Shanghai 200062, China
2 School of Communication and Electronic Engineering, East China Normal University, Shanghai 200062, China
3 School of Physics and Astronomy, and Tsung-Dao Lee Institute, Shanghai Jiao Tong University, Shanghai 200240, China
4 Shanghai Branch, Hefei National Laboratory, Shanghai 201315, China
5 Collaborative Innovation Center of Extreme Optics, Shanxi University, Taiyuan 030006, China
6 Shanghai Research Center for Quantum Science, Shanghai 201315, China
Corresponding authors. E-mail: †lqchen@phy.ecnu.edu.cn, ‡chyuan@phy.ecnu.edu.cn
Received December 21, 2024; accepted February 4, 2025

ABSTRACT

Due to the potential of quantum advantage to surpass the standard quantum limit (SQL), nonlinear interferometers have garnered significant attention from researchers in the field of precision measurement. However, many practical applications require multiparameter estimation. In this work, we discuss the precision limit of multi-parameter estimation of pure Gaussian states based on nonlinear interferometers, and derive the Holevo Cramér–Rao bound (HCRB) for the case where both modes undergo displacement estimation. Furthermore, we compare our analytical results with the quantum Cramér–Rao bound based on the symmetric logarithmic derivative (SLD-CRB), and with the result of the dual homodyne measurement. Through numerical analysis, we find that the HCRB equals the result of the dual homodyne measurement, whereas SLD-CRB is not saturable at small squeezed parameters. Therefore, this indicates that the HCRB is tight. Additionally, we provide intuitive analysis and visual representation of our numerical results in phase space.

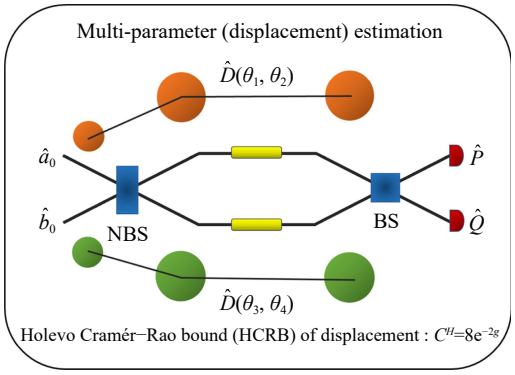

Keywords Holevo Cramér–Rao bound, nonlinear interferometers, multi-parameter estimation, dual homodyne measurement

1 Introduction

Precision measurement plays a crucial role in the research and development of physics, as it provides highly accurate measurement data. Interferometric measurement techniques, which rely on the interference phenomenon of waves to capture phase change information, are an indispensable tool for achieving high-precision measurements [1, 2]. This technique enables precise measurements of various physical quantities, such as angular velocity, magnetic field strength, and small distances. The phase measurement accuracy of traditional Mach–Zehnder interferometers (MZI) [3, 4] is limited by the standard quantum limit (SQL) [5, 6]. In 1986, Yurke *et al.* [7] proposed a new quantum interferometer scheme, the nonlinear SU(1,1) interferometer (SUI). Compared to traditional MZI, the SUI can achieve the Heisenberg limit (HL) with fewer optical components

Higher Education Press

https://doi.org/10.15302/frontphys.2025.032204

under appropriate quantum state injection [8–10].

Quantum metrology, a highly prominent research field today, focuses on utilizing unique quantum-enhanced effects to achieve ultra-high precision measurements for specific parameters. The core mission of this field is to surpass the SQL in traditional measurements through quantum systems, enabling high-precision parameter estimation [11–13]. Within this framework, quantum parameter estimation forms the theoretical foundation of quantum metrology, encompassing both single-parameter and multi-parameter estimation processes. To date, there has been a wealth of theoretical and experimental research on single-parameter estimation, accumulating substantial insights and practical experience [14–25]. In quantum parameter estimation, concepts such as the quantum Cramér–Rao bound based on the symmetric logarithmic derivative (SLD-CRB) [11] and quantum Fisher information (QFI) serve as crucial mathematical supports for single-parameter estimation research [26, 27].

However, it is worth noting that single-parameter estimation is often a simplified approach to complex real-world measurement models [28]. In most practical applications, joint estimation of multiple parameters is essential. To address this, the QFI has been extended to the quantum Fisher information matrix (QFIM), and the QCRB has been generalized to a matrix inequality form to meet the needs of multi-parameter estimation. However, in quantum mechanics, the non-commutativity of certain observables leads to the fact that the optimal measurement for a single parameter in multi-parameter estimation may become incompatible. This characteristic gives rise to new precision limits for multi-parameter estimation, such as the Cramér–Rao bound based on the right logarithmic derivative (RLD-CRB) [29, 30] and the Holevo Cramér–Rao bound (HCRB) [31].

Although the SLD-CRB and RLD-CRB provide valuable insights in some cases, they are generally not tight [32–34], and the SLD-CRB and RLD-CRB do not fully reflect the interdependencies between parameters, which limits their application in multi-parameter estimation with nonlinear interferometers. In contrast, HCRB represents a stricter bound and can be achieved in the asymptotic limit through collective measurements of a large number of states [35–38], and the difference between it and the SLD-CRB is bounded within a factor of two [32, 39], and it is asymptotically achievable under certain conditions [27, 40]. Compared to the SLD-CRB, the HCRB can more accurately reflect the practical scenario of multi-parameter estimation in nonlinear interferometers and can overcome the limitations of the SLD-CRB, providing a more reliable lower bound for parameter estimation precision. Therefore, the HCRB has higher practical and theoretical values in multi-parameter quantum estimation.

However, using the HCRB to assess parameter estimation precision involves more complex calculations than the RLD-CRB and SLD-CRB, mainly because the optimization process of the HCRB requires handling nonlinear functions in the Hermitian matrix space [41]. Under certain conditions, such as for Gaussian states [42–44], pure states [40, 45], estimation of qubit rotation [46, 47], qubit systems [48, 49], optical polarization [50], security issues in continuous-variable quantum communication protocols [51], and linear waveform estimation [52], the corresponding analytical expressions for the HCRB can be derived. However, for multi-parameter estimation problems in nonlinear interferometers, no related research has yet been conducted. This gap motivates the present work.

In this paper, we extend the method of Ref. [43] to the nonlinear interferometer model [53], considering the case where both modes experience unknown displacements. Based on the statistical model we establish, we derive the analytical expression for the HCRB and compute the results for the SLD-CRB. We evaluate and analyze the HCRB and SLD-CRB numerically, further verifying the effectiveness and accuracy of the HCRB. Additionally, we demonstrate through calculations that the theoretical limit of the dual homodyne measurement is consistent with the HCRB results. This outcome indicates that the dual homodyne measurement represents the optimal achievable measurement, confirming that the HCRB is tight. Finally, to provide a more intuitive presentation and analysis of our research results, we use phase-space images for visualization. The results of this study not only provide new theoretical support and technical methods for multi-parameter estimation in nonlinear interferometers, but also advance the field to a higher level.

The structure of our paper is as follows. In Section 2, we delve into the theory of multi-parameter quantum local estimation, which provides crucial theoretical support for our subsequent research. In Section 3, we describe in detail the measurement scheme for the displacement estimation of a two-mode Gaussian state based on a nonlinear interferometer, and the analytical expression of the HCRB has been derived. In Section 4, we compare the HCRB with SLD-CRB and the results from the dual homodyne measurement. We also use the numerical analysis and phase-space images to intuitively analyze and discuss our results. In Section 5, we summarize the paper and provide an outlook on future research directions.

2 Multi-parameter estimation theory

In this section, we give an overview of multi-parameter quantum estimation theory and its bounds including SLD-CRB, RLD-CRB and HCRB.

Consider a set of quantum states ρ_θ that encodes d

parameters, which can be represented as $\theta = (\theta_1, \theta_2, ..., \theta_d)$. Parameter estimation is performed by measuring the outcomes of ρ_θ to estimate the value of θ. In quantum mechanics, measurements are described by a set of positive operator-valued measures (POVM) $\hat{\Pi} = \{\hat{\Pi}_\chi\}$ [54], where each measurement outcome χ has a corresponding non-negative Hermitian operator $\hat{\Pi}_\chi$, and the POVM elements sum to Identity: $\sum_\chi \hat{\Pi}_\chi = I$. The probability of obtaining the measurement result χ when the state is ρ_θ is given by $p_\theta(\chi) = \mathrm{Tr}(\hat{\Pi}_\chi \rho_\theta)$. To obtain the estimated parameters based on the measurement result χ, we need an estimator $\hat{\theta}(\chi)$, which maps the measurement outcome χ to an estimate of θ. The accuracy of the estimator is typically assessed using its mean squared error (MSE) matrix, denoted by $V_\theta[\hat{\theta}]$, which is given by

$$V_\theta[\hat{\theta}] = \left[\sum_\chi p_\theta(\chi)\left(\hat{\theta}_j(\chi) - \theta_j\right)\left(\hat{\theta}_k(\chi) - \theta_k\right)\right]_{jk}. \quad (1)$$

An estimator is called a locally unbiased estimator if it satisfies $E\left[\hat{\theta}(\chi)\right] = \theta$ at the point θ. It is referred to simply as an unbiased estimator only if it is locally unbiased for all corresponding $\theta = (\theta_1, \theta_2, ..., \theta_d)$.

Assuming that M measurements are independent, the corresponding MSE matrix satisfies the Cramér–Rao bound (CRB), which provides a lower bound for the MSE matrix of a classical probability distribution $p_\theta(\chi)$:

$$V_\theta[\hat{\theta}] \geq \frac{1}{M} F^{-1}, \quad (2)$$

where F is the classical Fisher information (FI) matrix, defined as

$$F_{jk} = \sum_\chi p_\theta(\chi)\left(\partial_j \log p_\theta(\chi)\right)\left(\partial_k \log p_\theta(\chi)\right), \quad (3)$$

where $\partial_j = \frac{\partial}{\partial \theta_j}$. This holds for any fixed classical statistical model $p_\theta(\chi)$ [55]. For locally unbiased estimators, this bound is always achievable for any M. For more realistic estimators, this bound is obtained in the limit of infinite measurements M.

Due to this asymptotic achievability, especially when studying quantum applications, locally unbiased estimators are often used [27, 56], which corresponds to assuming that the number of repetitions M is sufficiently high to guarantee achievability. Therefore, in the following analysis, we can ignore the factor M from the expressions. Thus, by choosing suitable effective estimators, we can achieve at least the asymptotic CRB.

Moreover, quantum mechanics allows us to obtain a more general bound that depends solely on the quantum statistical model $p_\theta(\chi)$ and is independent of specific measurement strategies. Helstrom [57] introduced the SLD operator, while Yuen *et al.* [29] and Belavkin [30] introduced the RLD operator.

The SLD operator is implicitly defined by the following Lyapunov equation:

$$\frac{\partial \rho_\theta}{\partial \theta_i} = \frac{\rho_\theta L_i + L_i \rho_\theta}{2}. \quad (4)$$

For pure state models $\rho_\theta = |\psi_\theta\rangle\langle\psi_\theta|$, the above equation can be easily solved, yielding a simple form for the SLD operator:

$$L_i(\theta) = 2\frac{\partial \rho_\theta}{\partial \theta_i} = 2\left(|\psi_\theta\rangle\langle\partial_{\theta_i}\psi_\theta| + |\partial_{\theta_i}\psi_\theta\rangle\langle\psi_\theta|\right). \quad (5)$$

We can then define the entries of the QFIM in terms of the SLD operator as follows:

$$Q_{ij} = \mathrm{Tr}\left[\rho_\theta \frac{L_i L_j + L_j L_i}{2}\right]. \quad (6)$$

This can be used to derive a bound on the MSE, known as the SLD-CRB [26, 57], denoted as C_θ^S:

$$\nu \geq C_\theta^S = \mathrm{Tr}[Q_{ij}^{-1}]. \quad (7)$$

Another QCRB we consider is defined based on the RLD operator, which is given by

$$\frac{\partial \rho_\theta}{\partial \theta_i} = \rho_\theta L_i. \quad (8)$$

The entries of the QFIM in terms of the RLD operator are defined as

$$Q_{ij}^R = \mathrm{Tr}\left[\rho_\theta L_i L_j^\dagger\right]. \quad (9)$$

This leads to another bound on the MSE, known as the RLD-CRB [29], which we denote as C_θ^R:

$$\nu \geq C_\theta^R = \mathrm{Tr}\left\{\mathrm{Re}\left(Q^R\right)^{-1}\right\} + \mathrm{TrAbs}\left\{\mathrm{Im}\left(Q^R\right)^{-1}\right\}. \quad (10)$$

Here, $\mathrm{TrAbs}\{A\}$ denotes the sum of the absolute values of the eigenvalues of the matrix A. Although RLD-CRB and SLD-CRB are relatively easy to compute [14, 58], they are not always achievable.

Holevo derived another stricter bound for the MSE [27, 59], which we refer to as the HCRB. The HCRB is defined through the following minimization:

$$C_\theta^H := \min_{\vec{X} \in \chi} h_\theta[\hat{\boldsymbol{X}}]. \quad (11)$$

Here, $\hat{\boldsymbol{X}} = (\hat{X}_1, \hat{X}_2, ..., \hat{X}_d)$, and $\hat{X}_j$ is a Hermitian operator satisfying the following local unbiased constraint conditions:

$$\mathrm{Tr}(\rho_\theta \hat{X}_j) = 0, \quad (12)$$

$$\mathrm{Tr}\left(\frac{\partial \rho_\theta}{\partial \theta_j}\hat{X}_k\right) = \delta_{jk}. \quad (13)$$

Then,

$$h_\theta[\hat{\boldsymbol{X}}] := \mathrm{Tr}\{\mathrm{Re}Z_\theta[\hat{\boldsymbol{X}}]\} + \mathrm{TrAbs}\{\mathrm{Im}Z_\theta[\hat{\boldsymbol{X}}]\}, \tag{14}$$

where $Z_\theta[\hat{\boldsymbol{X}}]$ is a $d \times d$ matrix defined as

$$Z_\theta[\hat{\boldsymbol{X}}] := [\mathrm{Tr}(\rho_\theta \hat{X}_j \hat{X}_k)]_{j,k}. \tag{15}$$

For any Hermitian operator $\hat{\boldsymbol{X}}$ satisfying the local unbiased constraint conditions, we have $h_\theta[\hat{\boldsymbol{X}}] \geq C_\theta^S$ and $h_\theta[\hat{\boldsymbol{X}}] \geq C_\theta^H$. At the minimum of h_θ, we have $\nu \geq C_\theta^H$. Therefore, the HCRB is always greater than or equal to the SLD-CRB and RLD-CRB.

3 Precision bound-HCRB

In this section, we calculate the HCRB for the nonlinear interferometer model shown in Fig. 1. A coherent state $|\alpha\rangle$ and a vacuum state $|0\rangle$ are injected. Thus, the input state takes the form of

$$|\alpha, 0\rangle = \hat{D}(\alpha)\,|0, 0\rangle\,, \tag{16}$$

where $\hat{D}(\alpha)$ is the displacement operator for the coherent state, defined as

$$\hat{D}(\alpha) = \exp(\alpha \hat{a}_0^\dagger - \alpha^* \hat{a}_0). \tag{17}$$

After passing through the nonlinear beam splitter (NBS), which corresponds to the transformation induced by $\hat{U}_{NBS} = \exp(-\xi \hat{a}_0^\dagger \hat{b}_0^\dagger + \xi^* \hat{a}_0 \hat{b}_0)$, where $\xi = \eta \alpha_{pump}^2 t$, and t is the interaction time, the transformation of the annihilation operators is

$$\begin{pmatrix} \hat{a}_{out} \\ \hat{b}_{out} \end{pmatrix} = \begin{pmatrix} \cosh g & -\mathrm{e}^{\mathrm{i}\theta_g} \sinh g \\ -\mathrm{e}^{-\mathrm{i}\theta_g} \sinh g & \cosh g \end{pmatrix} \begin{pmatrix} \hat{a}_{in} \\ \hat{b}_{in} \end{pmatrix}, \tag{18}$$

where $\xi = g\mathrm{e}^{\mathrm{i}\theta_g}$ [60], g represents the strength of the nonlinear parametric process, and can also be referred to as the squeezed parameter. During the parameter encoding process after the NBS, the upper and lower arms of the interferometer undergo unknown displacements of $\hat{D}(\theta_1, \theta_2) = \exp(\mathrm{i}\theta_2 \hat{Q}_1 - \mathrm{i}\theta_1 \hat{P}_1)$ and $\hat{D}(\theta_3, \theta_4) = \exp(\mathrm{i}\theta_4 \hat{Q}_2 - \mathrm{i}\theta_3 \hat{P}_2)$ respectively. Here, $\hat{P}_i = (\hat{a}_i - \hat{a}_i^\dagger)/(2\mathrm{i})$ and $\hat{Q}_i = (\hat{a}_i + \hat{a}_i^\dagger)/2$ are a pair of orthogonal operators. After this, the corresponding state transforms into $|\psi\rangle$:

$$|\psi\rangle = \hat{D}(\theta_1, \theta_2)\hat{D}(\theta_3, \theta_4)\hat{U}_{NBS}\,|\alpha, 0\rangle\,. \tag{19}$$

Finally, after passing through a 50:50 beam splitter (BS), we note that the transformation associated with the BS is unitary. Therefore, passing through the BS will not affect the ultimate precision limit, and we can consider this process as part of the measurement scheme. After the BS, the state changes to $|\psi\rangle_{out}$:

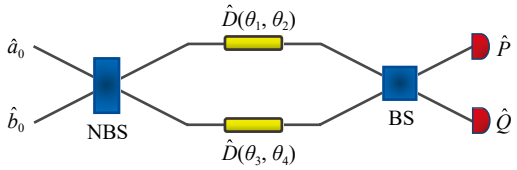

Fig. 1 Schematic of the nonlinear interferometers for displacement estimation. The two modes of the light field go through parameter encoding for unknown displacements after passing through the nonlinear beam splitter (NBS), then they mix at the beam splitter (BS), and finally, the dual homodyne measurement is performed on the output states. $\hat{a}_0$ and $\hat{b}_0$ represent the two modes of the light field in the interferometer.

$$\begin{aligned} |\psi\rangle_{out} &= \hat{U}_{BS}\hat{D}(\theta_1, \theta_2)\hat{D}(\theta_3, \theta_4)\hat{U}_{NBS}\,|\alpha, 0\rangle \\ &= \hat{D}'(\theta_1, \theta_2)\hat{D}'(\theta_3, \theta_4)\,|-\xi_{1a}, \alpha'\rangle\,|\xi_{1b}, \beta'\rangle\,, \end{aligned} \tag{20}$$

where $|-\xi_{1a}, \alpha'\rangle$ and $|\xi_{1b}, \beta'\rangle$ are two single-mode squeezed coherent states, $\hat{D}'(\theta_1, \theta_2)$ and $\hat{D}'(\theta_3, \theta_4)$ are the displacement operators after the BS transformation:

$$\begin{aligned} \hat{D}'(\theta_1, \theta_2) = \exp\Bigg(&\mathrm{i}\theta_2 \frac{1}{\sqrt{2}}\hat{Q}_1 - \mathrm{i}\theta_1 \frac{1}{\sqrt{2}}\hat{P}_1 \\ &+ \mathrm{i}\theta_2 \frac{1}{\sqrt{2}}\hat{Q}_2 - \mathrm{i}\theta_1 \frac{1}{\sqrt{2}}\hat{P}_2\Bigg), \end{aligned} \tag{21}$$

$$\begin{aligned} \hat{D}'(\theta_3, \theta_4) = \exp\Bigg(&\mathrm{i}\theta_4 \frac{1}{\sqrt{2}}\hat{Q}_2 - \mathrm{i}\theta_3 \frac{1}{\sqrt{2}}\hat{P}_2 \\ &- \mathrm{i}\theta_4 \frac{1}{\sqrt{2}}\hat{Q}_1 + \mathrm{i}\theta_3 \frac{1}{\sqrt{2}}\hat{P}_1\Bigg). \end{aligned} \tag{22}$$

The displacement operators $\hat{D}'(\theta_1, \theta_2)$ and $\hat{D}'(\theta_3, \theta_4)$ have the following partial derivatives with respect to $\theta_1, \theta_2, \theta_3$, and θ_4:

$$\begin{aligned} \partial_{\theta_1}\hat{D}'(\theta_1, \theta_2) &= \left(-\frac{\mathrm{i}}{\sqrt{2}}\hat{P}_1 - \frac{\mathrm{i}}{\sqrt{2}}\hat{P}_2 - \frac{\mathrm{i}}{4}\theta_2\right)\hat{D}'(\theta_1, \theta_2), \\ \partial_{\theta_2}\hat{D}'(\theta_1, \theta_2) &= \left(\frac{\mathrm{i}}{\sqrt{2}}\hat{Q}_1 + \frac{\mathrm{i}}{\sqrt{2}}\hat{Q}_2 + \frac{\mathrm{i}}{4}\theta_1\right)\hat{D}'(\theta_1, \theta_2), \\ \partial_{\theta_3}\hat{D}'(\theta_3, \theta_4) &= \left(-\frac{\mathrm{i}}{\sqrt{2}}\hat{P}_2 + \frac{\mathrm{i}}{\sqrt{2}}\hat{P}_1 - \frac{\mathrm{i}}{4}\theta_4\right)\hat{D}'(\theta_3, \theta_4), \\ \partial_{\theta_4}\hat{D}'(\theta_3, \theta_4) &= \left(\frac{\mathrm{i}}{\sqrt{2}}\hat{Q}_2 - \frac{\mathrm{i}}{\sqrt{2}}\hat{Q}_1 + \frac{\mathrm{i}}{4}\theta_3\right)\hat{D}'(\theta_3, \theta_4). \end{aligned} \tag{23}$$

To simplify the calculation, we compute the HCRB when θ is small. Thus, we evaluate it at $\theta = 0$, because the bounds for all θ values are the same. The reason we can do this is that the HCRB is asymptotically achievable under adaptive measurement schemes, given a set of n identical states $\rho_\theta^{\otimes n}$, where $n \to \infty$. By using $\sqrt{n}$ states for a small number of measurements, a rough estimate of θ can be obtained, after which the remaining $n - \sqrt{n}$

states can be replaced by $D(-\tilde{\theta})$, where $\tilde{\theta}$ is the rough estimate of θ, resulting in the state for small θ.

Next, we compute $|\psi\rangle_{out}$ and the partial derivatives of $|\psi\rangle_{out}$ with respect to θ_1, θ_2, θ_3, and θ_4 when $\theta_i = 0$:

$$\begin{aligned}
|\psi_0\rangle &= |\psi\rangle_{out}|_{\theta=0} = |-\xi_{1a}, \alpha'\rangle\,|\xi_{1b}, \beta'\rangle\,,\\
|\psi_1\rangle &= \partial_{\theta_1}|\psi\rangle_{out}|_{\theta=0}\\
&= -\frac{\mathrm{i}}{\sqrt{2}}[\hat{P}_1\,|-\xi_{1a}, \alpha'\rangle\,|\xi_{1b}, \beta'\rangle + \hat{P}_2\,|-\xi_{1a}, \alpha'\rangle\,|\xi_{1b}, \beta'\rangle],\\
|\psi_2\rangle &= \partial_{\theta_2}|\psi\rangle_{out}|_{\theta=0}\\
&= \frac{\mathrm{i}}{\sqrt{2}}[\hat{Q}_1\,|-\xi_{1a}, \alpha'\rangle\,|\xi_{1b}, \beta'\rangle + \hat{Q}_2\,|-\xi_{1a}, \alpha'\rangle\,|\xi_{1b}, \beta'\rangle],\\
|\psi_3\rangle &= \partial_{\theta_3}|\psi\rangle_{out}|_{\theta=0}\\
&= -\frac{\mathrm{i}}{\sqrt{2}}[\hat{P}_2\,|-\xi_{1a}, \alpha'\rangle\,|\xi_{1b}, \beta'\rangle - \hat{P}_1\,|-\xi_{1a}, \alpha'\rangle\,|\xi_{1b}, \beta'\rangle],\\
|\psi_4\rangle &= \partial_{\theta_4}|\psi\rangle_{out}|_{\theta=0}\\
&= \frac{\mathrm{i}}{\sqrt{2}}[\hat{Q}_2\,|-\xi_{1a}, \alpha'\rangle\,|\xi_{1b}, \beta'\rangle - \hat{Q}_1\,|-\xi_{1a}, \alpha'\rangle\,|\xi_{1b}, \beta'\rangle].
\end{aligned} \tag{24}$$

We are interested in the inner products of $|\psi_0\rangle$, $|\psi_1\rangle$, $|\psi_2\rangle$, $|\psi_3\rangle$, and $|\psi_4\rangle$. We set the coherent state corresponding to $\theta_\alpha = 0$, and set $\theta'_g = \pi/2$ for the NBS process, where $\theta_\alpha = 0$ means that α is a real number. Under these circumstances, we present the results of the calculations of five relevant inner products as follows:

$$\langle\psi_0|\psi_0\rangle = 1,\ \langle\psi_0|\psi_1\rangle = -\mathrm{i}|\alpha|\cosh(g), \tag{25}$$

$$\langle\psi_0|\psi_2\rangle = \langle\psi_0|\psi_4\rangle = 0,\ \langle\psi_0|\psi_3\rangle = -\mathrm{i}|\alpha|\sinh(g). \tag{26}$$

We introduce a set of standard orthogonal basis states $\{|e_0\rangle, |e_1\rangle, |e_2\rangle\}$ that satisfy the corresponding inner product conditions:

$$\begin{aligned}
|\psi_0\rangle &= |e_0\rangle,\\
|\psi_1\rangle &= -\mathrm{i}|\alpha|\cosh(g)|e_0\rangle + \frac{\mathrm{i}\sinh(g)}{2}|e_1\rangle - \frac{\mathrm{i}\cosh(g)}{2}|e_2\rangle,\\
|\psi_2\rangle &= \frac{-\sinh(g)}{2}|e_1\rangle - \frac{\cosh(g)}{2}|e_2\rangle,\\
|\psi_3\rangle &= -\mathrm{i}|\alpha|\sinh(g)|e_0\rangle + \frac{\mathrm{i}\cosh(g)}{2}|e_1\rangle - \frac{\mathrm{i}\sinh(g)}{2}|e_2\rangle,\\
|\psi_4\rangle &= \frac{\cosh(g)}{2}|e_1\rangle + \frac{\sinh(g)}{2}|e_2\rangle.
\end{aligned} \tag{27}$$

According to the local unbiased constraint condition in Eqs. (12) and (13), they can be written as the following two equations:

$$\langle e_0|\hat{X}_1|e_0\rangle = \langle e_0|\hat{X}_2|e_0\rangle = \langle e_0|\hat{X}_3|e_0\rangle = \langle e_0|\hat{X}_4|e_0\rangle = 0, \tag{28}$$

and

$$\langle\psi_0|\hat{X}_k|\psi_j\rangle + \langle\psi_0|\hat{X}_k|\psi_j\rangle = \delta_{jk},\ j,k = 1,2,3,4. \tag{29}$$

In Eq. (29), each Hermitian operator $\hat{X}_j$ is subject to four conditions, and there are a total of sixteen constraints.

To find the HCRB, we need to minimize the expression in Eq. (11). Thus, we can set the components of $\hat{X}_1, \hat{X}_2, \hat{X}_3$, and $\hat{X}_4$ that do not involve the above twenty constraints to their complex conjugates. We define the components using their real and imaginary parts:

$$\begin{aligned}
&\langle e_0|\hat{X}_1|e_1\rangle = t_1 + \mathrm{i}j_1,\ \langle e_0|\hat{X}_1|e_2\rangle = s_1 + \mathrm{i}k_1,\\
&\langle e_0|\hat{X}_2|e_1\rangle = t_2 + \mathrm{i}j_2,\ \langle e_0|\hat{X}_2|e_2\rangle = s_2 + \mathrm{i}k_2,\\
&\langle e_0|\hat{X}_3|e_1\rangle = t_3 + \mathrm{i}j_3,\ \langle e_0|\hat{X}_3|e_2\rangle = s_3 + \mathrm{i}k_3,\\
&\langle e_0|\hat{X}_4|e_1\rangle = t_4 + \mathrm{i}j_4,\ \langle e_0|\hat{X}_4|e_2\rangle = s_4 + \mathrm{i}k_4.
\end{aligned} \tag{30}$$

The matrix in Eq. (15) is given by

$$Z_\theta[\hat{\boldsymbol{X}}] = \begin{pmatrix}
\mathrm{tr}(\rho_\theta\hat{X}_1\hat{X}_1) & \mathrm{tr}(\rho_\theta\hat{X}_1\hat{X}_2) & \mathrm{tr}(\rho_\theta\hat{X}_1\hat{X}_3) & \mathrm{tr}(\rho_\theta\hat{X}_1\hat{X}_4)\\
\mathrm{tr}(\rho_\theta\hat{X}_2\hat{X}_1) & \mathrm{tr}(\rho_\theta\hat{X}_2\hat{X}_2) & \mathrm{tr}(\rho_\theta\hat{X}_2\hat{X}_3) & \mathrm{tr}(\rho_\theta\hat{X}_2\hat{X}_4)\\
\mathrm{tr}(\rho_\theta\hat{X}_3\hat{X}_1) & \mathrm{tr}(\rho_\theta\hat{X}_3\hat{X}_2) & \mathrm{tr}(\rho_\theta\hat{X}_3\hat{X}_3) & \mathrm{tr}(\rho_\theta\hat{X}_3\hat{X}_4)\\
\mathrm{tr}(\rho_\theta\hat{X}_4\hat{X}_1) & \mathrm{tr}(\rho_\theta\hat{X}_4\hat{X}_2) & \mathrm{tr}(\rho_\theta\hat{X}_4\hat{X}_3) & \mathrm{tr}(\rho_\theta\hat{X}_4\hat{X}_4)
\end{pmatrix}. \tag{31}$$

Using the matrix $Z_\theta[\hat{\boldsymbol{X}}]$, we can compute the function $h_\theta[\hat{\boldsymbol{X}}]$, and minimizing it leads to the HCRB result, given as

$$C^H = 8\mathrm{e}^{-2g}. \tag{32}$$

From the above expression, we find that the value of the HCRB decreases as the squeezed parameter g increases.

4 Discussion

In this section, we make a comparison between the analytical results of HCRB and SLD-CRB, as well as the results from the dual homodyne measurement.

4.1 SLD-CRB

Based on the partial derivatives of the displacement operators with respect to the parameters to be estimated, we can calculate the partial derivatives of $|\psi\rangle_{out}$ with respect to the parameters. Substituting these expressions into the definition of the SLD operator given in Eq. (5), we find the following SLD operators:

$$\begin{aligned}
L_1(\theta) &= 2\left(|\psi_0\rangle\langle\psi_1| + |\psi_1\rangle\langle\psi_0|\right),\\
L_2(\theta) &= 2\left(|\psi_0\rangle\langle\psi_2| + |\psi_2\rangle\langle\psi_0|\right),\\
L_3(\theta) &= 2\left(|\psi_0\rangle\langle\psi_3| + |\psi_3\rangle\langle\psi_0|\right),\\
L_4(\theta) &= 2\left(|\psi_0\rangle\langle\psi_4| + |\psi_4\rangle\langle\psi_0|\right).
\end{aligned} \tag{33}$$

Next, using the definition from Eq. (6), we can derive the QFI matrix. After some calculations, we get the

following diagonal matrix:

$$Q^S = \begin{pmatrix} \cosh(2g) & 0 & 0 & 0 \\ 0 & \cosh(2g) & 0 & 0 \\ 0 & 0 & \cosh(2g) & 0 \\ 0 & 0 & 0 & \cosh(2g) \end{pmatrix}. \tag{34}$$

Finally, according to the definition given in Eq. (7), we can determine the corresponding SLD-CRB as follows:

$$C^S = \mathrm{Tr}\left[(Q^S)^{-1}\right] = \frac{4}{\cosh(2g)}. \tag{35}$$

From this expression, we see that under this statistical model, as the squeezed parameter g increases, the value of SLD-CRB decreases. Therefore, in scenarios where only displacement estimation is involved, squeezing is a valuable resource for improving the precision of displacement estimation. The larger the squeezed parameter, the better the overall estimation precision that can be achieved.

4.2 Dual homodyne measurement

By examining the equations corresponding to the statistical model in Eq. (20), we find that both modes carry information about the displacement. Thus, when the two modes pass through a BS and are squeezed in orthogonal directions in phase space, we can optimally estimate the corresponding encoded parameters by performing appropriate orthogonal measurements on the output modes. The dual homodyne measurement scheme requires homodyne measurement of the orthogonal components of the two modes separately, so from Eq. (3), we can derive the corresponding FI matrix as follows:

$$F = \frac{1}{2}\begin{pmatrix} \mathrm{e}^{2g} & 0 & 0 & 0 \\ 0 & \mathrm{e}^{2g} & 0 & 0 \\ 0 & 0 & \mathrm{e}^{2g} & 0 \\ 0 & 0 & 0 & \mathrm{e}^{2g} \end{pmatrix}. \tag{36}$$

Therefore, the estimated precision from the dual homodyne measurement is

$$C^F = \mathrm{Tr}[F^{-1}] = 8\mathrm{e}^{-2g}. \tag{37}$$

This result indicates that this bound is consistent with our previously obtained HCRB result. Since the dual homodyne measurement scheme is the optimal measurement scheme for our statistical model, we conclude that the HCRB is indeed tight.

As shown in Fig. 2, the results of the HCRB, SLD-CRB, and the sum of the MSE for the dual homodyne measurement as a function of the squeezed parameter g are shown. We can see that both the HCRB and SLD-CRB values decrease as the squeezed parameter g increases, indicating that squeezing is a useful resource for enhancing the precision of displacement estimation. Since the dual homodyne measurement is the optimal measurement strategy, we find that the value of HCRB is equal to that of the dual homodyne measurement, which demonstrates that HCRB is tight. Furthermore, the HCRB value is greater than that of SLD-CRB when the squeezed parameter g is relatively small, indicating that using HCRB for evaluation is superior to SLD-CRB. As the squeezed parameter g increases beyond a certain point, the values of both bounds converge.

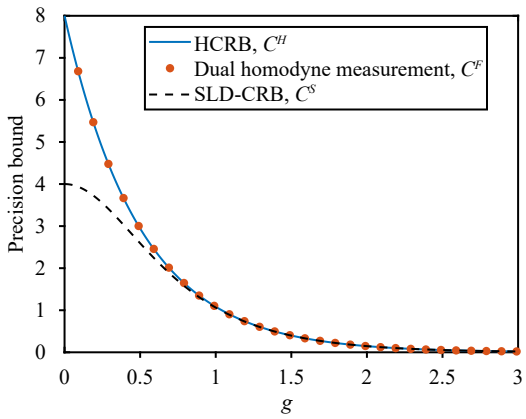

Fig. 2 Precision bound as a function of squeezed parameter g. The black dashed line represents the result of SLD-CRB, the blue solid line shows the HCRB and the orange dotted line represents estimation precision obtained using the dual homodyne measurement scheme. The diagram shows that the HCRB is consistent with the estimation precision achieved by the dual homodyne measurement scheme.

Next, we provide an intuitive analysis and visualization of our numerical results by illustrating the corresponding phase space diagrams of our statistical model in different processes. The input states of the vacuum state and the coherent state can be represented by the yellow solid circle and the blue solid circle at the bottom, respectively, in the phase diagram of Fig. 3. Since we set $\theta_\alpha = 0$ for the coherent state, the corresponding phase diagram for the coherent state lies along the axis where $p = 0$. After passing through the NBS, entangled two-mode squeezed light is generated. To facilitate our description in phase space, we consider the phase diagram of a single mode, where the individual mode distribution of a two-mode squeezed state follows a thermal distribution. The slightly larger solid yellow and blue circles in the middle of Fig. 3 indicate that the fluctuations of the orthogonal components of each mode have increased after passing through the NBS, resulting in the larger circles in phase space. Finally, after displacement encoding, the phase diagrams corresponding to the two modes have unknown displacements in phase space. Based on the phase diagram, we can explain why the results we derived concerning HCRB and SLD-CRB do not include terms related to the number of photons.

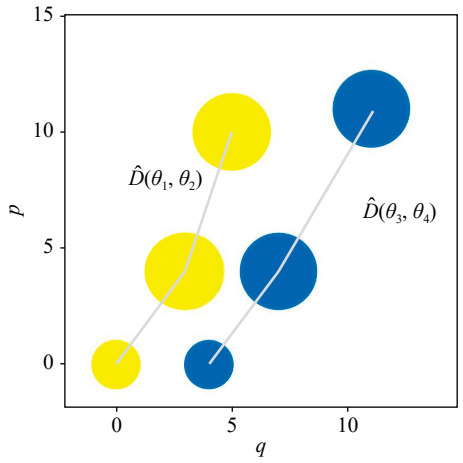

Fig. 3 Phase space evolution of the two-mode light field after passing through the interferometer. The three yellow circles on the left correspond to the transformations of mode $\hat{a}_0$ in the interferometer, while the three blue circles on the right correspond to the transformations of mode $\hat{b}_0$. The two smallest circles at the bottom represent the vacuum state and the coherent state. The two relatively larger circles in the middle and the two circles at the top respectively represent the phase space images of the light field after undergoing the NBS and the displacement encoding process.

This is because we can treat the displacement throughout the process and the unknown encoded displacement as a unified entity. When discussing the corresponding limits of estimation accuracy, the fluctuations in the Orthogonal components remain unchanged. Consequently, when we are only interested in displacement estimation, the resulting precision limits do not involve terms with photon numbers.

5 Conclusion

In summary, we have provided a method for calculating the HCRB and analyzed the estimation problem under the injection of coherent and vacuum states into a nonlinear interferometer, followed by unknown displacement encoding. We have derived the analytical expression for the HCRB corresponding to the statistical model, and discussed its dependence on the squeezed parameter g. Our findings indicate that squeezing contributes to enhancing the HCRB, and that the HCRB results are superior to those of SLD-CRB, demonstrating that HCRB is tight.

These results may offer methods for further improving measurement precision and achieving practically reliable detection schemes. Currently, our derivation focuses on the parameter estimation problem for an ideal nonlinear interferometer with Gaussian pure state inputs. Our next step will involve extending this methodology to investigate related estimation issues concerning Gaussian mixed states in the presence of photon loss.

Declarations The authors declare that they have no competing interests and there are no conflicts.

Acknowledgements This work was supported by the Shanghai Science and Technology Innovation Project (No. 24LZ1400600), the Innovation Program for Quantum Science and Technology (No. 2021ZD0303200), the National Natural Science Foundation of China (Grant Nos. U23A2075, 12274132, 11974111, 12234014, 11654005, 11874152, and 91536114), Shanghai Municipal Science and Technology Major Project (Grant No. 2019SHZDZX01), Innovation Program of Shanghai Municipal Education Commission (No. 202101070008E00099), the National Key Research and Development Program of China (Grant No. 2016YFA0302001), and Fundamental Research Funds for the Central Universities. W. Z. acknowledges additional support from the Shanghai Talent Program.

References

1. A. A. Michelson and E. W. Morley, On the relative motion of the earth and the luminiferous ether, *Am. J. Sci.* s3-34(203), 333 (1887)
2. A. R. Thompson, J. M. Moran, and G. W. Swenson, Interferometry and Synthesis in Radio Astronomy, Springer Nature, 2017
3. L. Zehnder, Ein neuer interferenzrefraktor, *Zeitschrift für Instrumentenkunde* 11, 275 (1891)
4. L. Mach, Ueber einen interferenzrefraktor, *Zeitschrift für Instrumentenkunde* 12, 89 (1892)
5. S. L. Braunstein, Quantum limits on precision measurements of phase, *Phys. Rev. Lett.* 69(25), 3598 (1992)
6. V. Giovannetti, S. Lloyd, and L. Maccone, Quantum metrology, *Phys. Rev. Lett.* 96(1), 010401 (2006)
7. B. Yurke, S. L. McCall, and J. R. Klauder, Su(2) and SU(1, 1) interferometers, *Phys. Rev. A* 33(6), 4033 (1986)
8. F. Hudelist, J. Kong, C. Liu, J. Jing, Z. Ou, and W. Zhang, Quantum metrology with parametric amplifier-based photon correlation interferometers, *Nat. Commun.* 5(1), 3049 (2014)
9. D. Li, C. H. Yuan, Z. Ou, and W. Zhang, The phase sensitivity of an SU(1, 1) interferometer with coherent and squeezed-vacuum light, *New J. Phys.* 16(7), 073020 (2014)
10. D. Li, B. T. Gard, Y. Gao, C. H. Yuan, W. Zhang, H. Lee, and J. P. Dowling, Phase sensitivity at the Heisenberg limit in an SU(1, 1) interferometer via parity detection, *Phys. Rev. A* 94(6), 063840 (2016)
11. S. L. Braunstein and C. M. Caves, Statistical distance and the geometry of quantum states, *Phys. Rev. Lett.* 72(22), 3439 (1994)
12. V. Giovannetti, S. Lloyd, and L. Maccone, Quantum-enhanced measurements: Beating the standard quantum limit, *Science* 306(5700), 1330 (2004)
13. V. Giovannetti, S. Lloyd, and L. Maccone, Advances in quantum metrology, *Nat. Photonics* 5(4), 222 (2011)
14. M. G. Paris, Quantum estimation for quantum technol-

ogy, *Int. J. Quant. Inf.* 7(Supp01), 125 (2009)
15. F. Albarelli, M. Barbieri, M. G. Genoni, and I. Gianani, A perspective on multiparameter quantum metrology: From theoretical tools to applications in quantum imaging, *Phys. Lett. A* 384(12), 126311 (2020)
16. J. Sahota and D. F. James, Quantum-enhanced phase estimation with an amplified Bell state, *Phys. Rev. A* 88(6), 063820 (2013)
17. Y. Watanabe, T. Sagawa, and M. Ueda, Optimal measurement on noisy quantum systems, *Phys. Rev. Lett.* 104(2), 020401 (2010)
18. S. Z. Ang, G. I. Harris, W. P. Bowen, and M. Tsang, Optomechanical parameter estimation, *New J. Phys.* 15(10), 103028 (2013)
19. A. Monras and F. Illuminati, Information geometry of gaussian channels, *Phys. Rev. A* 81(6), 062326 (2010)
20. M. D. Lang and C. M. Caves, Optimal quantum-enhanced interferometry, *Phys. Rev. A* 90(2), 025802 (2014)
21. H. Yuan, Sequential feedback scheme outperforms the parallel scheme for Hamiltonian parameter estimation, *Phys. Rev. Lett.* 117(16), 160801 (2016)
22. P. Kok, J. Dunningham, and J. F. Ralph, Role of entanglement in calibrating optical quantum gyroscopes, *Phys. Rev. A* 95(1), 012326 (2017)
23. M. Jarzyna and R. Demkowicz-Dobrzanski, Quantum interferometry with and without an external phase reference, *Phys. Rev. A* 85(1), 011801 (2012)
24. M. Takeoka, K. P. Seshadreesan, C. You, S. Izumi, and J. P. Dowling, Fundamental precision limit of a Mach–Zehnder interferometric sensor when one of the inputs is the vacuum, *Phys. Rev. A* 96(5), 052118 (2017)
25. C. You, S. Adhikari, X. Ma, M. Sasaki, M. Takeoka, and J. P. Dowling, Conclusive precision bounds for SU(1, 1) interferometers, *Phys. Rev. A* 99(4), 042122 (2019)
26. C. W. Helstrom, Quantum detection and estimation theory, *J. Stat. Phys.* 1(2), 231 (1969)
27. A. S. Holevo, Probabilistic and Statistical Aspects of Quantum Theory, Vol. 1, Springer Science & Business Media, 2011
28. M. Szczykulska, T. Baumgratz, and A. Datta, Multiparameter quantum metrology, *Adv. Phys. X* 1(4), 621 (2016)
29. H. Yuen and M. Lax, Multiple-parameter quantum estimation and measurement of non-self-adjoint observables, *IEEE Trans. Inf. Theory* 19(6), 740 (1973)
30. V. P. Belavkin, Generalized uncertainty relations and efficient measurements in quantum systems, arXiv: quant-ph/0412030 (2004)
31. A. S. Holevo, Statistical decision theory for quantum systems, *J. Multivariate Anal.* 3(4), 337 (1973)
32. A. Carollo, B. Spagnolo, A. A. Dubkov, and D. Valenti, On quantumness in multi-parameter quantum estimation, *J. Stat. Mech.* 2019(9), 094010 (2019)
33. S. Razavian, M. G. Paris, and M. G. Genoni, On the quantumness of multiparameter estimation problems for qubit systems, *Entropy (Basel)* 22(11), 1197 (2020)
34. A. Candeloro, M. G. Paris, and M. G. Genoni, On the properties of the asymptotic incompatibility measure in multiparameter quantum estimation, *J. Phys. A* 54(48), 485301 (2021)
35. S. Massar and S. Popescu, Optimal extraction of information from finite quantum ensembles, *Phys. Rev. Lett.* 74(8), 1259 (1995)
36. J. Kahn and M. Guta, Local asymptotic normality for finite dimensional quantum systems, *Commun. Math. Phys.* 289(2), 597 (2009)
37. K. Yamagata, A. Fujiwara, and R. D. Gill, Quantum local asymptotic normality based on a new quantum likelihood ratio, *Ann. Stat.* 41(4), 2197 (2013)
38. Y. Yang, G. Chiribella, and M. Hayashi, Attaining the ultimate precision limit in quantum state estimation, *Commun. Math. Phys.* 368(1), 223 (2019)
39. M. Tsang, F. Albarelli, and A. Datta, Quantum semiparametric estimation, *Phys. Rev. X* 10(3), 031023 (2020)
40. K. Matsumoto, A new approach to the Cramér–Rao-type bound of the pure-state model, *J. Phys. Math. Gen.* 35(13), 3111 (2002)
41. F. Albarelli, J. F. Friel, and A. Datta, Evaluating the Holevo Cramér–Rao bound for multiparameter quantum metrology, *Phys. Rev. Lett.* 123(20), 200503 (2019)
42. M. Bradshaw, P. K. Lam, and S. M. Assad, Ultimate precision of joint quadrature parameter estimation with a gaussian probe, *Phys. Rev. A* 97(1), 012106 (2018)
43. M. Bradshaw, S. M. Assad, and P. K. Lam, A tight Cramér–Rao bound for joint parameter estimation with a pure two-mode squeezed probe, *Phys. Lett. A* 381(32), 2598 (2017)
44. G. Bressanini, M. G. Genoni, M. Kim, and M. G. Paris, Multi-parameter quantum estimation of single- and two-mode pure gaussian states, *J. Phys. A* 57(31), 315305 (2024)
45. A. Fujiwara and H. Nagaoka, Quantum fisher metric and estimation for pure state models, *Phys. Lett. A* 201(2–3), 119 (1995)
46. L. O. Conlon, J. Suzuki, P. K. Lam, and S. M. Assad, Efficient computation of the Nagaoka–Hayashi bound for multiparameter estimation with separable measurements, *npj Quantum Inf.* 7, 110 (2021)
47. L. O. Conlon, P. K. Lam, and S. M. Assad, Multiparameter estimation with two-qubit probes in noisy channels, *Entropy (Basel)* 25(8), 1122 (2023)
48. J. Suzuki, Explicit formula for the Holevo bound for two-parameter qubit-state estimation problem, *J. Math. Phys.* 57(4), 042201 (2016)
49. S. K. Yung, L. O. Conlon, J. Zhao, P. K. Lam, and S. M. Assad, Comparison of estimation limits for quantum two-parameter estimation, *Phys. Rev. Res.* 6(3), 033315 (2024)
50. M. Jarzyna, Quantum limits to polarization measurement of classical light, in: *Quantum 2.0*, Optica Publishing Group, 2022, pp QW2A–39
51. L. O. Conlon, B. Shajilal, A. Walsh, J. Zhao, J. Janousek, P. K. Lam, and S. M. Assad, Verifying the security of a continuous variable quantum communication protocol via quantum metrology, *npj Quantum Inf.* 10, 35 (2024)
52. J. W. Gardner, T. Gefen, S. A. Haine, J. J. Hope, and Y. Chen, Achieving the fundamental quantum limit of

linear waveform estimation, *Phys. Rev. Lett.* 132(13), 130801 (2024)
53. J. Kong, Z. Ou, and W. Zhang, Phase-measurement sensitivity beyond the standard quantum limit in an interferometer consisting of a parametric amplifier and a beam splitter, *Phys. Rev. A* 87(2), 023825 (2013)
54. M. A. Nielsen and I. L. Chuang, Quantum Computation and Quantum Information, Cambridge University Press, 2010
55. H. Cramer, Mathematical Methods of Statistics, Vol. 26, Princeton University Press, 1999
56. J. Suzuki, Y. Yang, and M. Hayashi, Quantum state estimation with nuisance parameters, *J. Phys. A Math. Theor.* 53(45), 453001 (2020)
57. C. W. Helstrom, Minimum mean-squared error of estimates in quantum statistics, *Phys. Lett. A* 25(2), 101 (1967)
58. D. Petz and C. Ghinea, Introduction to quantum fisher information, in: Quantum Probability and Related Topics, World Scientific, 2011, pp 261–281
59. A. S. Holevo, Noncommutative analogues of the Cramér–Rao inequality in the quantum measurement theory, in: Proceedings of the Third Japan—USSR Symposium on Probability Theory, Springer, 2006, pp 194–222
60. Q. K. Gong, X. L. Hu, D. Li, C. H. Yuan, Z. Ou, and W. Zhang, Intramode-correlation-enhanced phase sensitivities in an SU(1, 1) interferometer, *Phys. Rev. A* 96(3), 033809 (2017)